Gravitational waves from hidden sectors.

Pascos 2024, Quy Nhon, Vietnam

July 7-13, 2024

PN

Northeastern University, Boston, Massachusetts, USA.

July7-14

Topics

- Gravitational waves (GW) and fundamental physics.
- A strong GW signal requires BSM physics such as those involving hidden sectors.

  This talk will be focussed mostly on gravitational waves from hidden sectors using first order phase transition (FOPT).

  However, a cosmologically consistent model of GW from hidden sector must also include the SM sector.
- Bubble nucleation in a two-field analysis.
- Gravitational wave power spectrum
  - Effect of the speed of sound on GW power spectrum.
  - Imprint of nucleation modes (detonation, deflagration, hybrid) on the power spectrum.
  - Theory reach and current/proposed experiments.

Gravitational waves and fundamental physics

The observation of gravitational waves in black hole mergers in 2016 [1] opened up a new avenue to explore fundamental physics.

- There are various possible sources of gravitational waves
  - Compact binary inspiral gravitational waves (LIGO).
  - Continuous GW (from spinning neutron stars).
  - GWs from Gamma Ray Bursts (GRB's) and possibly from other sources of unknown origin.
  - Stochastic GW.
- Stochastic GW could reveal fundamental new physics
  - Inflation, Big Bang.
  - Cosmic strings, primordial black hole evaporation.
  - **Cosmic phase transitions, specifically First Order Phase Transition (FOPT).**

[1] B. P. Abbott *et al.* [LIGO Scientific and Virgo], Phys. Rev. Lett. **116**, no.6, 061102 (2016).

FOPT[2]: standard model vs experiment.

- Standard model does not produce a strong enough gravitational wave measurable by current/proposed detectors.

$$\Omega_{GW} h^2 \leq 10^{-28} \qquad \text{(reach of standard model)}.$$

$$\Omega_{GW} h^2 \geq 10^{-20} \qquad \text{(reach of proposed detectors)}.$$

- Hidden sectors could provide much larger gravitational waves possibly in the observational range.

[2] D. A. Kirzhnits, JETP Lett. **15**, 529-531 (1972)
D. A. Kirzhnits and A. D. Linde, Phys. Lett. B **42**, 471-474 (1972)
M. Kamionkowski, A. Kosowsky and M. S. Turner, Phys. Rev. D **49**, 2837-2851 (1994)

Hidden sectors

- In a large class of BSM models such as extra dimension models (such as SUGRA and string models, D-brane models, moose/quiver models) there exist hidden sectors which can connect with the visible sector via a wide variety of portals.
  - Higgs portal [3]
  - Kinetic mixing [4]
  - Stueckelberg mass mixing [5]
  - Kinetic-Stueckelberg mixing [6], Stueckelberg-Higgs mixing[7]
  - Higher dimensional operators such as $\frac{\lambda}{M^d} O_{vis} O_{hid}$ [8]
- In the analysis of FOPT using hidden sectors one must also include the SM for cosmological consistency.

[3] B. Patt and F. Wilczek, [arXiv:hep-ph/0605188 [hep-ph]].
[4] B. Holdom, Phys. Lett. B **166**, 196-198 (1986)
[5] B. Kors and PN, Phys. Lett. B **586**, 366-372 (2004).
[6] D. Feldman, Z. Liu and PN, Phys. Rev. D **75**, 115001 (2007).
[7] M. Du, Z. Liu and PN, Phys. Lett. B **834**, 137454 (2022).
[8] PN, Phys. Rev. Lett. **76**, 2218-2221 (1996).

The GW analysis needs to be cosmologically consistent

Most of the analyses on GW using just the hidden sector appear not to be cosmologically consistent. There are several reasons:

- One obvious reason is that the hidden and the visible sectors are entangled via the hubble expansion
$$H^2 = (8\pi G/3)(\rho_{vis}(T) + \rho_{hid}(T_h)).$$
- The strength of the phase transition $\alpha = \epsilon/\rho_{rad}$ where ϵ is the latent heat and $\rho_{rad} = \rho^{rad}_{vis}(T) + \rho^{rad}_{hid}(T_h)$.
- In general the hidden and the visible sectors are in different temperatures a meaningful analysis requires a knowedge of $\xi(T)$ where
$$\xi(T) = \frac{T_h}{T}.$$
- Imposition of ΔN_{eff} constraint at T(BBN) requires knowledge of T_h since
$$\Delta N_{eff} \propto (T_h/T)^4.$$

Cosmologically consistent analysis of hidden and visible sectors

- The cosmologically consistent approach for synchronous evolution of the visible and the hidden sectors involves use of energy conservation equations [9]

$$\frac{d\rho_v}{dt} + 3H(\rho_v + p_v) = j_v, \quad \text{visible}\,,$$
$$\frac{d\rho_h}{dt} + 3H(\rho_h + p_h) = j_h, \quad \text{hidden}\,,$$

  where j_v and j_h are the sources.

- Using the energy conservation equation, one can derive an equation for the evolution function $\xi(T) = T_h/T$.

$$\frac{d\xi}{dT} = \left[-\xi\frac{d\rho_h}{dT_h} + \frac{4H\zeta_h\rho_h - j_h}{4H\zeta\rho - 4H\zeta_h\rho_h + j_h}\frac{d\rho_v}{dT}\right](T\frac{d\rho_h}{dT_h})^{-1}.$$

  Here $\zeta = 1$ (radiation dominance), $\zeta = 3/4$ (matter dominance).

[9] A. Aboubrahim and PN, JHEP **09**, 084 (2022).
A. Aboubrahim, W. Z. Feng, PN and Z. Y. Wang, Phys. Rev. D **103**, no.7, 075014 (2021).

Separate entropy conservation for visible/hidden sectors to estimate ξ is a bad approximation [10]

$\boldsymbol{\xi(T)}$ vs $\boldsymbol{T}$ for various $\boldsymbol{\xi_0}$.

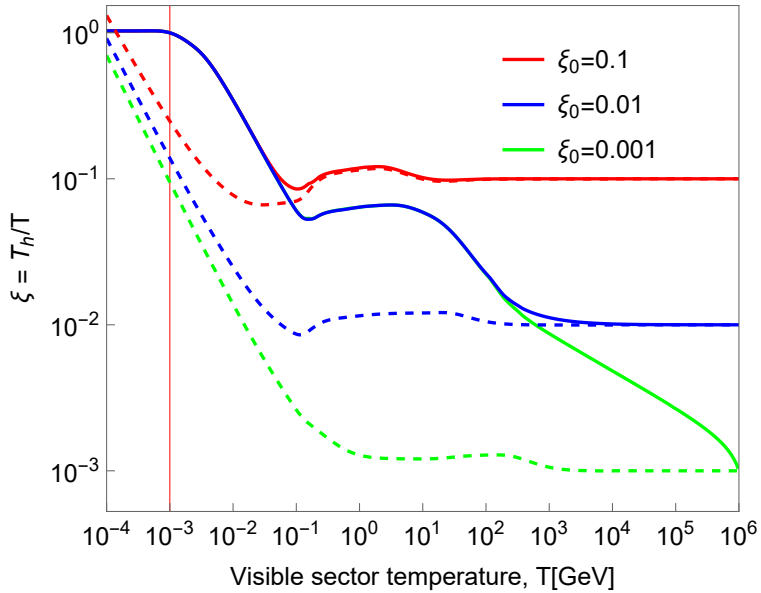

Caption: An analysis of $\boldsymbol{\xi(T)}$ vs $\boldsymbol{T}$ for $\boldsymbol{\xi_0 = 0.1, 0.01, 0.001}$ and kinetic mixing $\boldsymbol{\delta = 4 \times 10^{-8}}$. Solid curves are using synchronous evolution while dashed curves are using separate entropy conservation for the hidden and the visible sector.

The analysis shows that the use of separate entropy conservation in hidden & visible sectors is a bad approximation even for feeble couplings between the visible & hidden sectors.

[10] J. Li and PN, Phys. Rev. D **108**, no.11, 115008 (2023).

A hidden sector model coupled to SM for GW analysis[11]

- The model consists of SM and a hidden sector which is charged under a $U(1)_X$ gauge symmetry with field content: A_μ (gauge field), D (Dirac fermion), Φ (complex scalar) and a kinetic energy portal $\frac{\delta}{2} A_{\mu\nu} B^{\mu\nu}$.

- We study a first order phase transition involving the SM and the hidden sector and is governed by the tree potential $V = V_{0sm} + V_{oh}$

$$V_{0h} = -\mu_h^2 \Phi\Phi^* + \lambda_h (\Phi^*\Phi)^2,$$
$$\Phi = \frac{1}{\sqrt{2}}(\chi_c + \chi + iG_h^0); \quad G_h^0 : \text{Goldstone}$$

$$m_A^2(\chi_c) = g_x^2 \chi_c^2,\ m^2(\chi_c) = -\mu_h^2 + 3\lambda_h \chi_c^2,\ m_{G_h^0}^2(\chi_c) = -\mu_h^2 + \lambda_h \chi_c^2.$$

The field dependent masses become temperature dependent in a thermal field theory[12]

[11] W. Feng, J. Li and PN, [arXiv:2403.09558 [hep-ph]] .

[12] S. Weinberg, Phys. Rev. D **9**, 3357-3378 (1974).
L. Dolan and R. Jackiw, Phys. Rev. D **9**, 3320-3341 (1974).

- The potential governing the FOPT involves, tree, the zero-temperature 1-loop Coleman-Weinberg potential, and the one loop thermal potential, and daisy diagrams[13]

$$\mathbf{V_{eff}^{h}(\Phi, T_h) = V_{0h} + V_{1h}^{(0)} + \Delta V_{1h}^{(T_h)} + V_h^{daisy}(T_h)\,,}$$

$$\mathbf{\Delta V_{1h}^{(T_h)}(\chi_c, T_h) = \sum_i g_i \int_0^\infty dq\, q^2 \ln\left[1 \mp \exp\left(-\sqrt{q^2 + m_i^2/T_h^2}\right)\right],\quad i = (B, F)\,.}$$

- The daisy loop contributions are only for the longitudinal mode of vector and the scalars. The temperature dependent potential is given by

$$\mathbf{V^{daisy}(i, T_h) = -\frac{T_h}{12\pi}\left\{\left[m_i^2 + \Pi_i(T_h)\right]^{3/2} - m_i^3\right\}.}$$

Here $\mathbf{\Pi_i(T_h)}$ is the thermal contribution to the zero temperature mass $\mathbf{m_i^2}$ arising from "daisy" diagrams and known as the "Debye mass". It can be computed using Matsubara and Kubo-Martin-Schwinger imaginary time formalism[14]

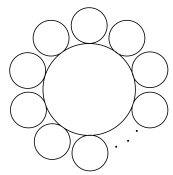

[13] W. Feng, J. Li and PN, [arXiv:2403.09558 [hep-ph]] .

[14] T. Matsubara, Prog. Theor. Phys. **14**, 351-378 (1955); R. Kubo, J. Phys. Soc. Japan 12 (1957) 570; P.C. Martin and J. Schwinger, Phys. Rev. 115 (1959) 1342.

Nucleation and vacuum decay: one field case

- At zero temperature the vacuum decay probability per unit time and per unit volume is $\boldsymbol{\Gamma = Ke^{-S_4}}$ where $\boldsymbol{S_4}$ Euclidean action in 4-d and $\boldsymbol{K}$ is proportional to fourth power of energy in the phase transition.
- At finite temperature $\boldsymbol{\Gamma = K(T)e^{-S_3/T}}$, $\boldsymbol{K(T) \sim T^4}$ and

$$\boldsymbol{S_3(T) = \int_0^\infty 4\pi r^2 dr \left[\frac{1}{2}\left(\frac{d\phi}{dr}\right)^2 + V^v_{\rm eff}(\phi, T)\right]}\ .$$

with the scalar field satisfying the Euclidean O(3) symmetry equation of motion and the appropriate boundary conditions

$$\boldsymbol{\frac{d^2\phi}{dr^2} + \frac{2}{r}\frac{d\phi}{dr} = \frac{\partial}{\partial\phi}V^v_{\rm eff}(\phi, T), \quad \lim_{r\to\infty}\phi = 0, \quad \frac{d\phi}{dr}\,|_{r=0} = 0,}$$

- Tunneling temperature $\boldsymbol{T_n}$

$$\boldsymbol{\int_0^{T_n} \frac{\Gamma dt}{H^3} = \int_{T_n}^\infty \frac{dT}{T}\left(\frac{90}{8\pi^3 g_{eff}}\right)^2\left(\frac{M_{Pl}}{T}\right)^4 e^{-S_3(T)/T} \simeq 1.}$$

For two field nucleation with ϕ (visible) and χ(hidden)

We assume no interaction between the two scalar fields in the potential. In this case there will be two types of non-interaction bubbles: one for the visible sector and the other for the hidden sector. Here $S_{3total}(T)$ is given by

$$S_{3total}(T) = S_{3v}(T) + S_{3h}(\xi(T)T)$$

Here the equations of motion are to be solved with Euclidean $O(3)$ symmetry and with appropriate boundary conditions for each field. In this case nucleation for the combined system happens at $T_{n,total}$

$$\frac{S_{3\text{toal}}(T_{n,total})}{T_{n,total}} = \frac{S_{3\text{v}}(T_{n,total})}{T_{n,total}} + \frac{S_{3\text{h}}(\xi(T_{n,total})T_{n,total})}{T_{n,total}} \sim 140 \qquad (1)$$

which tells us that $\frac{S_{3\text{v}}(T_{n,total})}{T_{n,total}} < 140$. However, S_{3v}/T is a monotonic increasing function of T which leads to

$$\exists\, T_n > T_{n,total} : \frac{S_{3\text{v}}(T_n)}{T_n} \sim 140 \qquad (2)$$

It tells us that before the original false vacuum decays directly into the final true vacuum, it must decay into an intermediate vacuum first.

Extension to two field tunneling: SM Higgs and hidden scalar [15]

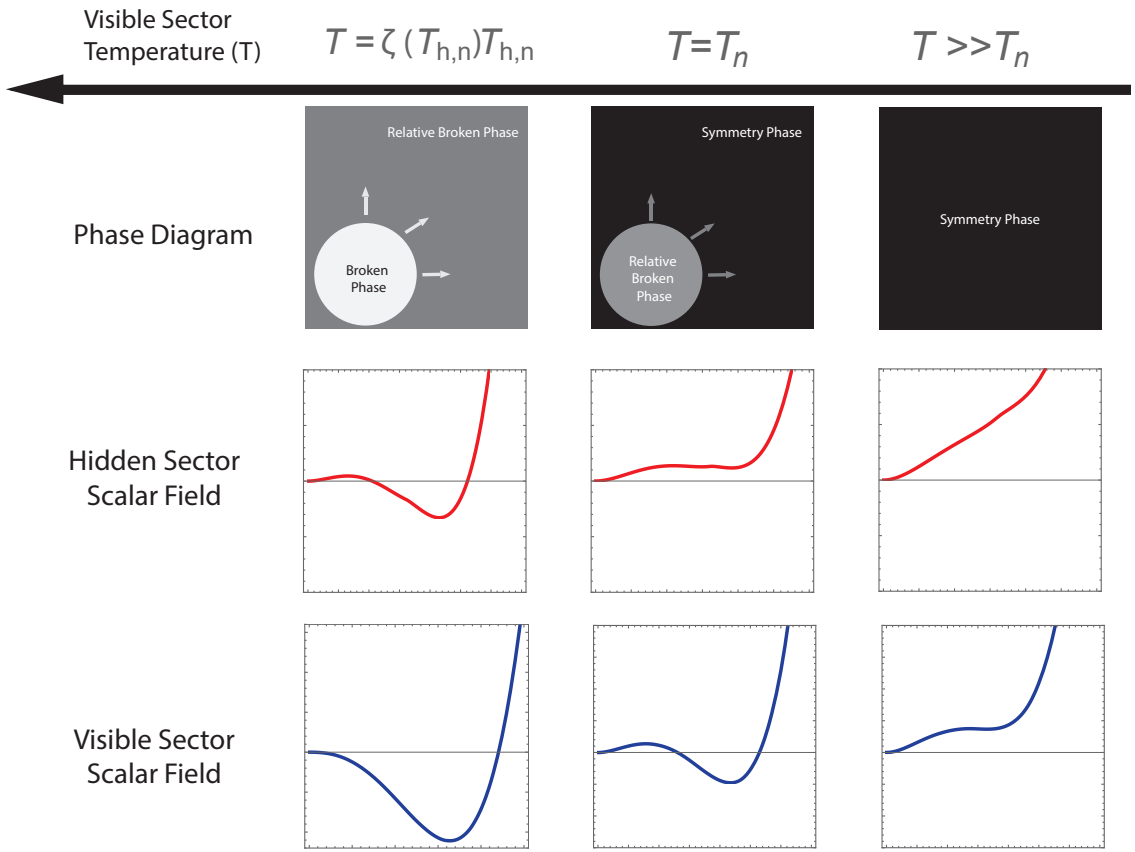

The phase of the whole universe transfers from the symmetry phase to the relative broken phase before ultimately reaching the fully broken phase. The plots of $\boldsymbol{V_{\text{eff}}^{\text{v}}}$ v.s. $\boldsymbol{\phi}$ and $\boldsymbol{V_{\text{eff}}^{\text{h}}}$ v.s. $\boldsymbol{\chi}$ are shown for different temperatures.

[15] W. Feng, J. Li and PN, [arXiv:2403.09558 [hep-ph]] .

The strength of phase transition depends on the speed of sound

- In general sound speed depends on whether the medium is in the symmetric phase $(+)$ or broken phase $(-)$ and also depends on the visible and the hidden sector temperature, i.e., $\boldsymbol{c_s^2 = (\phi_v, \chi_h, T, T_h)}$.
- Four different sound velocities that enter in the analysis
  - Visible sector nucleation: $\boldsymbol{c_s^2(+, v)}$, $\boldsymbol{c_s^2(-, v)}$
  - Hidden sector nucleation: $\boldsymbol{c_s^2(+, h)}$, $\boldsymbol{c_s^2(-, h)}$.
- In most analyses of first order phase transition, sound velocities are treated approximately often assuming $\boldsymbol{c_{s,-}^2 = c_{s,+}^2 = \frac{1}{3}}$. In this case the phase transition strength $\boldsymbol{\alpha}$ is given by

$$\boldsymbol{\alpha = \frac{T\frac{d\Delta V_{eff}}{dT} - \Delta V_{eff}}{\rho_{rad}}.}$$

- In our analysis[16] we have taken into account the dependence of $\boldsymbol{\alpha}$ on sound velocity[17]. The expression for $\boldsymbol{\alpha}$ is too long to display, and it will be indicated with a subscript, i.e., $\boldsymbol{\alpha_{\bar{\theta}}}$.

[16] W. Feng, J. Li and PN, [arXiv:2403.09558 [hep-ph]].
F. Giese, T. Konstandin, K. Schmitz and J. van de Vis, JCAP **01**, 072 (2021).

[17] $\boldsymbol{c_s^2 = dp/de}$, $\boldsymbol{e = T(\partial p/\partial T) - p}$.

Nucleation modes: Detonation, deflagration, hybrid

In the analysis [18] we have used Chapman-Jouguet velocity [19] in part to distinguish different bubble nucleation modes [20]

$$v_J = \frac{1 + \sqrt{3\alpha_{\bar{\theta}}(1 - c_s^2 + 3c_s^2\alpha_{\bar{\theta}})}}{1/c_s + 3c_s\alpha_{\bar{\theta}}}.$$

For $i = v, h$

1. Detonations: $v_w > c_s(-, i)$ and $v_w > v_J$, (Wall velocity v_w is supersonic.)
2. Deflagrations: $v_w < c_s(-, i)$ (Wall velocity v_w is subsonic.)
3. Hybrid: $v_w > c_s(-, i)$ and $v_w < v_J$ (In between case.)

---

[18] W. Feng, J. Li and PN, [arXiv:2403.09558 [hep-ph]].

[19] L. D. Landau and E. M. Lifshitz, *Fluid Mechanics*, 2nd edition, (Pergamon Press, Oxford, 1989)
R. Courant and K. O. Friedrichs, *Supersonic Flow and Shock Waves* (Springer-Verlag, Berlin, 1985)
M. Laine,"Bubble growth as a detonation," Phys. Rev. D **49**, 3847-3853 (1994)

[20] F. Giese, T. Konstandin, K. Schmitz and J. van de Vis, JCAP **01**, 072 (2021)

Gravitational power spectrum Ω_{GW}

- The phase transition and the power spectrum depends on several parameters: T_n, α, β, v_w, κ among others. α controls the strength of the phase transition and β the duration of the transition $\beta \simeq \frac{1}{\Gamma}\frac{d\Gamma}{dt}\Big|_{t=t_n}$.

$$\Omega_{\rm GW}(f) = \frac{1}{\rho_c}\frac{d\rho_{\rm GW}}{d\ln f} \simeq \mathcal{N}\Delta\left(\frac{\kappa\alpha}{1+\alpha}\right)^p\left(\frac{H}{\beta}\right)^q s(f),$$

$$\Omega_{\rm GW} \simeq \Omega_{\rm sw} + \Omega_{\rm tb}.$$

κ (efficiency factor) is the fraction of the latent heat converted into gravitational waves.

$\Omega_{\rm type}$:	$\mathcal{N}$	κ	p	q	Δ	f_p	$s(f)$
Ω_{sw} :	0.159	κ_{sw}	2	1	v_w	$\frac{2\beta}{\sqrt{3}v_w}$	$(f/f_p)^3\left(\frac{7}{4+3f/f_p)^2}\right)^{7/2}$
Ω_{turb} :	20.1	$\epsilon_{turb}\kappa_{sw}$	$\frac{3}{2}$	1	v_w	$\frac{3.5\beta}{2v_w}$	$\frac{(f/f_p)^3}{(1+f/f_p)^{11/3}(1+8\pi f/H)}$

Inclusion of redshift from tunneling temperature T_n to current temperature T_0

$$\Omega_{GW}(f) \leftrightarrow (\frac{a}{a_0})^4(\frac{H}{H_0})^2\Omega_{GW}(\frac{a_0}{a}f)$$

Contributions of sound waves and turbulence to the power spectrum [21]

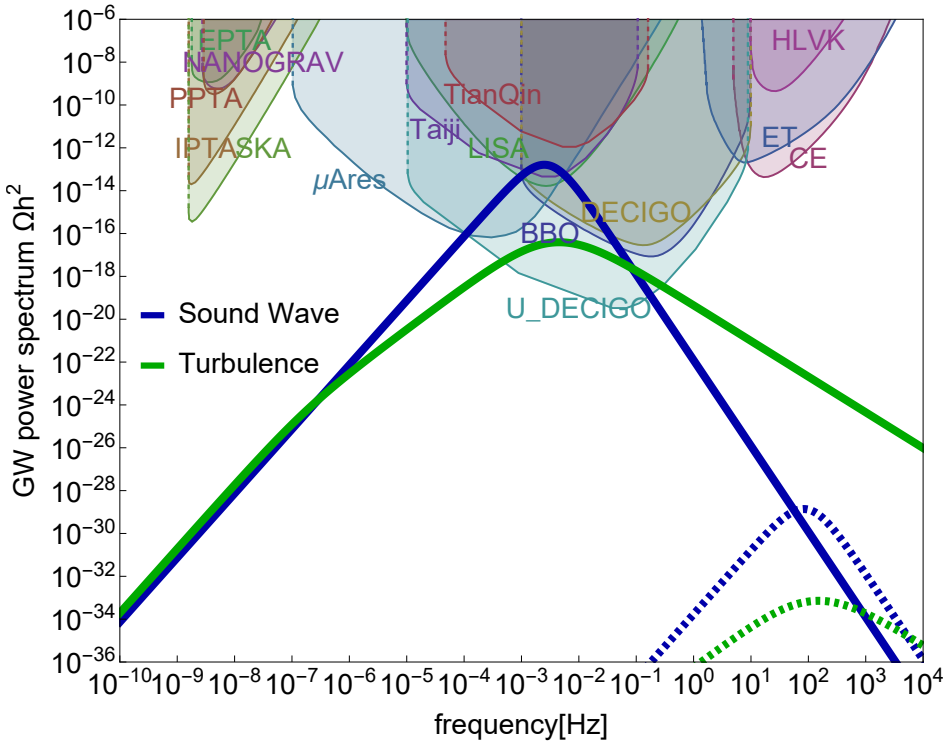

Solid lines: Hidden sector. Dashed lines: Visible sector. $\epsilon_{\mathbf{turb}} = \mathbf{0.1}$.

[21] W. Feng, J. Li and PN, [arXiv:2403.09558 [hep-ph]].

Sensitivity of GW power spectrum to the speed of sound [22]

- Case A: $c_s^2 = 1/3$ [23].
- Case B: Effect of hidden sector sound speed on $\Omega_{GW}h^2$.
- Case C: Effect of hidden and visible sector sound speeds on $\Omega_{GW}h^2$.

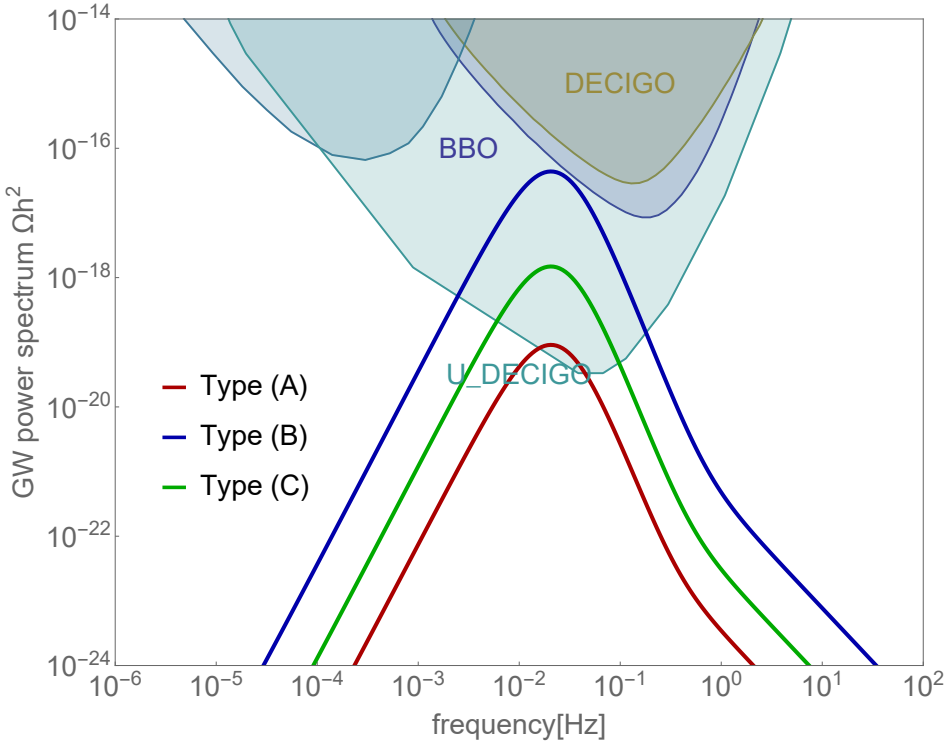

$c_s^2(-, h) = 0.333$ (A: −); 0.234 (B: −); 0.309 (C:−).

[22] W. Feng, J. Li and PN, [arXiv:2403.09558 [hep-ph]] (To appear in PRD).

[23] L. D. Landau and E. M. Lifshitz, *Fluid Mechanics*, 2nd edition, (Pergamon Press, Oxford, 1989)

Imprint of nucleation modes on power spectrum [24]

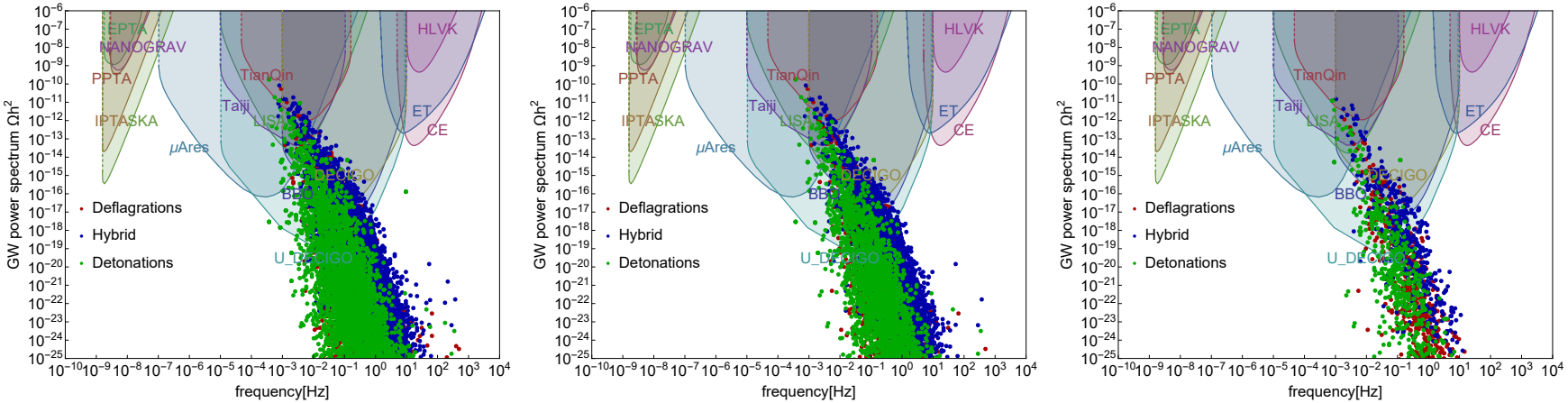

Green: Detonation; Blue: Hybrid; Red: Deflgration.

- Left panel: allowed set of models satisfying the FOPT constraints.
- Middle panel: same as the left panel with models satisfying FOPT constraints and the $\boldsymbol{\Delta N_{\rm eff}}$ constraint.
- Right: residual set of models satisfying the FOPT constraint, $\boldsymbol{\Delta N_{\rm eff}}$ constraint and the relic density constraint.

[24] W. Feng, J. Li and PN,[arXiv:2403.09558 [hep-ph]] (To appear in PRD).

Conclusion

- Study of gravitational waves opens up a new avenue for the exploration of fundamental physics on the interface of particle physics and cosmology.
- Detection of stochastic gravitational waves may reveal the dynamics of bubble formation and reveal the early history of the universe.
- While CMB allows us to explore the universe some 300,000 yrs ago, gravitational waves from the Big Bang can allow us to look back at times as early as $\simeq \mathbf{10^{-30}}$ s.
- There is no other experiment that holds that possibility. Thus it is of great interest to build gravitational detectors with sensitivities in the frequency over as wide a range as possible to understand the early history of the universe.

Gravitational wave detectors

- The gravitational wave detectors currently in operation are: LIGO, Virgo, KAGRA.
- Detectors at the proposal/beginning stage:
  - LISA: (Laser Interferometer Space Antenna): Collaboration of European Space Agency (ESA) and US NASA. Mid -2030 launch.
  - Einstein Telescope: European, ground based.
  - Cosmic Explorer (CE): US, ground based.
  - TianQin: China, space based.
  - Taiji: China, space based.
  - DECIGO: Japanese, space based.